Computational Rim Illumination with Aerial Robots

Manohar Srikanth*
MIT

Kavita Bala†
Cornell University

Frédo Durand‡
MIT

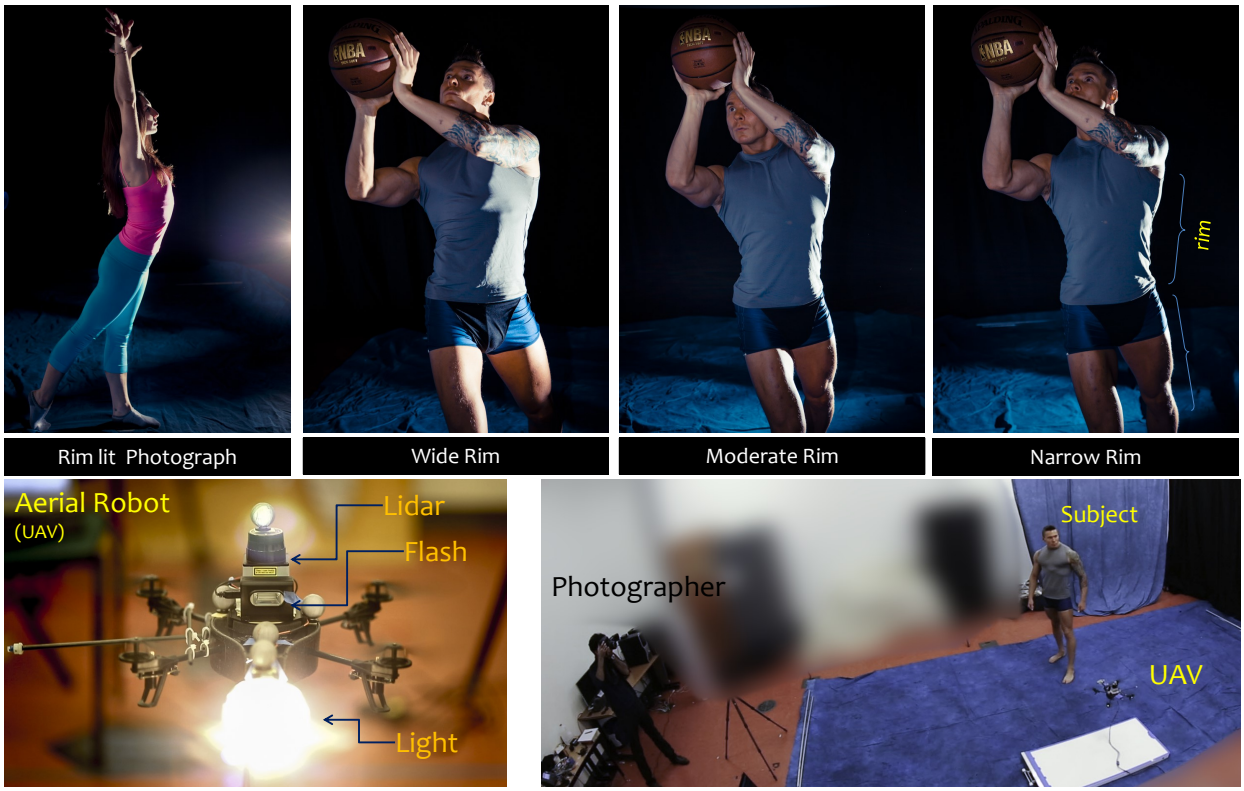

Figure 1: *By analyzing the images from the photographer's camera, an aerial robot carrying a light source automatically guides itself to a lighting location to achieve a desired rim-lit photograph. Top row: results with various specified rim width values. Bottom-Left: Our aerial robot, a quadrotor aerial robot equipped with a flash, continuous light source, and a Lidar to detect and follow a moving subject. Bottom-right: Our photography setup showing the subject, aerial robot and the photographer.*

Abstract

Lighting plays a major role in photography. Professional photographers use elaborate installations to light their subjects and achieve sophisticated styles. However, lighting moving subjects performing dynamic tasks presents significant challenges and requires expensive manual intervention. A skilled additional assistant might be needed to reposition lights as the subject changes pose or moves, and the extra logistics significantly raises costs and time.

We present a new approach to lighting dynamic subjects where an aerial robot equipped with a portable light source lights the subject to automatically achieve a desired lighting effect. We focus on rim lighting, a particularly challenging effect to achieve with dynamic subjects, and allow the photographer to specify a required rim width. Our algorithm processes the images from the photographer's camera and provides necessary motion commands to the aerial robot to achieve the desired rim width in the resulting photographs. We demonstrate a control approach that localizes the aerial robot with reference to the subject and tracks the subject to achieve the necessary motion. Our proof-of-concept results demonstrate the utility of robots in computational lighting.

CR Categories: I.2.10 [Vision and Scene Understanding]: Intensity, color, photometry, and thresholding— [I.4.1]: Digitization and Image Capture—Scanning I.2.9 [Robotics]: Autonomous vehicles—Commercial robots and applicationsKinematics and dynamics;

Keywords: Computational Photography, Lighting, Localization

1 Introduction

Lighting plays a critical role in good photography. Through the careful placement of lights, photographers can define space and enhance the mood of photographs. Perhaps the most dramatic example is the use of a rim light behind the subject, which highlights

*e-mail:srimano@alum.mit.edu
†e-mail:kb@cs.cornell.edu
‡e-mail:fredo@csail.mit.edu

silhouettes and can be used as the main light for silhouetted styles, or as an accent to separate a subject from the background. Rim lighting effects are usually associated with posed studio photography because they require the careful placement of lights relative to a static subject and often involve a whole crew where assistants move the lights until the photographer is satisfied with the look of the image. Photographers increasingly try to push the envelope and deal with dynamic scenarios by having assistants track a moving subject, but this remains costly, challenging, and might require many takes. There are two central challenges in rim lighting for photography of dynamic scenes: the ability to move the lights (usually handled by assistants), and the decision of how to move them, usually made by the photographer based on what he or she sees in the viewfinder.

In this paper we propose an automated technique for rim lighting in dynamic settings with moving subjects. We combine the use of computational photography and robotically-controlled light source to facilitate the use of advanced lighting effects such as rim lighting for moving subjects. Our vision is that light sources should be actuated and be able to react to movements in the scene based on feedback from the main camera to achieve a lighting specified by the photographer. In particular, we leverage recent advances in aerial robotics and their commoditization, to enable the full 3D placement of light sources around the subject. We focus on the case of rim lighting because it is particularly challenging, important for artistic control, and requires precise positioning of lights.

In our scenario, the photographer holds a main camera with the goal of capturing a picture of a potentially-moving subject. The photographer controls a desired rim width as a function of the look they want to achieve. An aerial robot (also known as unmanned aerial vehicles, or UAVs) is responsible for the rim light and reacts to the movements of the photographer and the subject to automatically position the rim light to achieve the desired rim width. The photographer can also specify a wider or thinner rim width and the aerial robot responds accordingly. We introduce a simple computational measure of rim width from the image seen by the photographer's camera. While this quantitative rim width is not intended to be a direct characterization of aesthetics, it provides easy control for the photographer who can increase it or decrease it until they achieve a desired look.

To enable the automatic placement of rim lights, we introduce a new aerial robot control strategy based not only on absolute localization and sensors on the aerial robot, but also on a computational characterization of rim lighting from the main camera. At a very high level, our control strategy moves the robot away from the photographer (behind the subject) to make the rim thinner, and closer to make it wider. We focus on the placement of the robot within a given horizontal plane because it is the most critical degree of freedom for rim lighting human subjects, but a similar strategy could be used to also modulate the altitude of the aerial robot. In addition to rim width, our controller needs to achieve a number of other objectives such as respecting a given distance to the subject, keeping the robot at a given height, and making sure that the light carried by the robot is directed towards the subject. Figure 1 top row shows our results for various rim widths.

We demonstrate our approach with a prototype that relies on a small quadrotor aerial robot that weighs less than one pound (see Figure 1, bottom left). The aerial robot we use is a low cost (about $300), lightweight quadrotor [Parrot 2010; Bristeau et al. 2011] that can easily carry a standard flash as well as a lidar unit (about $2,000) to help track the subject. The Lidar can easily be replaced with a cheaper alternative like Kinect sensor. We show that the system is able to automatically adjust to subject movement and to free photographers from the labor of lighting placement, enabling free-form photography while achieving a desired rim lighting.

This paper makes the following contributions:

- We demonstrate the first approach for studio-quality lighting using aerial robots.
- We introduce a control approach based on a combination of rim computation from the perspective of the camera and tracking of the subject from the aerial robot.

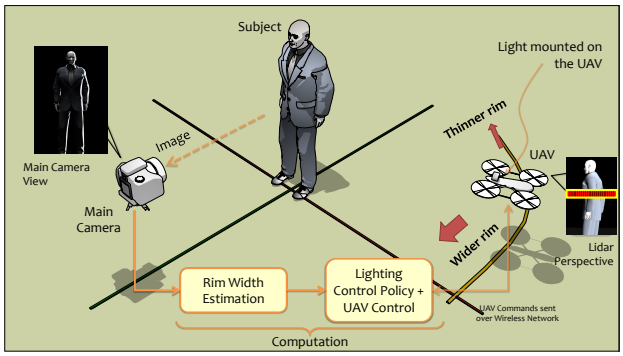

Figure 2: *System Overview: The photographer shoots the subject with the main camera; an aerial robot, a quadrotor, equipped with a light source illuminates the subject from the side as shown. The video images from the main camera are analyzed to evaluate the quality of rim light and consequently, the robot position is continuously adjusted to achieve a desired quality of rim light effect. Positioning the robot closer to the side of the subject produces a "wider" rim light effect, while positioning it behind the subject leads to "thinner" rim light effect.*

2 Related work

Our work is focused on closed-loop real-time computational illumination of real life objects for photographic purposes. We briefly review papers on computational illumination of both real objects and computer graphic object (where the geometry is known).

Computational Illumination: [Petschnigg et al. 2004; Eisemann and Durand 2004] propose methods to computationally combine two photographs, captured with and without an on-camera flash, so as to improve the overall illumination of the scene. [Raskar et al. 2004] proposes to combine multiple photographs, each taken with a different light position, to generate non-photorealistic image.

[Debevec et al. 2002] introduced the light stage, a dome with hundreds of light that can achieve arbitrary lighting of a dynamic subject to match a given characteristic. The main drawbacks of such an approach being cost and portability. [Anrys et al. 2004] proposes to arrange a set of fixed lights around a near-diffuse static object whose intensities are to be determined. Using an image-based user interface, the user is allowed to express the desired lighting characteristics. [Mohan et al. 2005] proposes a mechanical rotating light system that is used to capture a number of images of a static scene with various lighting conditions. With a user interface, they combine images to generate desired lighting effect. In [Wang et al. 2010], the authors propose a realtime feedback system to light a dynamics scene in order to emphasize certain characteristics of the scene (for instance the edges of the objects). The main goal here is to better visualize the actual scene rather than obtaining an optimally lit photograph. Their system relies on optically aligned camera and projector through a beam splitter, and shared light spectrum (IR and visible light). More recent work [Boyadzhiev et al. 2013] uses several flash photographs of a static scene captured from the same view point with varying light positions. They combine

the images, with some user inputs, to produce a composite that has a desired lighting characteristics. Obviously, this approach is well suited for static scenes, for instance architectural photography. Moreover, the capture process is not well guided or automated (except for photographer's own experience), and the photographer may end up capturing far more photographs, often containing redundant information.

Lighting design in Computer Graphics: [Bousseau et al. 2011] synthesize an optimal lighting environment map that enhances the appearance of scene objects from a given viewpoint. They use an image quality metric, and knowledge of the scene geometry and material properties to design the optimal environment map. [Pellacini et al. 2007] proposes an iterative system where the user specifies the desired scene lighting by means of light painting the surface of the 3D objects. They then solve for the light parameters that achieve the desired look. [Akers et al. 2003] present methods to enhance rendering by changing lighting. They propose the use of rim lighting as a way to highlight the silhouette of a 3D model. [Schoeneman et al. 1993] presents painting with light, which attempts to solve an inverse problem. Given a desired appearance of the scene that has fixed light sources, they solve for the color and the intensity of the light sources. [Poulin and Fournier 1992] propose using highlights and shadows as a user specified input; they then solve for the optimal lighting parameters.

In contrast to the above, our work is focused on real-time lighting optimization of real life dynamic objects. We use a robotic platform that responds to the motion of the subject and photographer in order to maintain a desired lighting effect. To make the robot respond quickly, we design an efficient control system for the robot. Hence, understanding and using the dynamics of the robot becomes an integral part of the problem.

Quadrotor Aerial Robot: A quadrotor aerial robot, also known as an unmanned aerial vehicle, is capable of complex flight motion, and is also capable of hovering at a fixed location in 3D space. Aerial robots are routinely used to carry a camera in photography and filmography. To our best knowledge, application of an aerial robot to carry a light source for photographic purposes is novel. In addition, using feedback to correct and optimize the robots position ishacked2001automatics also novel.

3 Overview

The photographer aims the camera at the subject, while an aerial robot equipped with a light source hovers near the subject to provide rim lighting. Our algorithm analyzes the images from the camera to evaluate the rim lighting. Given a desired rim-width as specified by the photographer, our guidance policy determines the direction of motion of the robot (hence the light), so as to achieve the desired rim-width. Our real-time control loop ensures quick adaptation to the changes in the subject position and posture, as well as to the changes in the position of the photographer.

The aerial robot, is a standard off-the-shelf quadrotor and its four propellers provide four controllable degrees of freedom: xyz-position, and rotation about its own vertical z-axis (also called yaw angle). The tilt angles (roll and pitch) are internally used for controlling the lateral xy position of the robot: when the robot is tilted, its dynamics moves it along the corresponding horizontal direction.

We use a continuous light source and a flash strobe on the aerial robot, and both are assumed to be spot lights. The continuous light is used during the process of robot position optimization, during which it should be the dominant light source. The onboard flash strobe is triggered only at the time of capturing the final still photograph, and additional light sources can be fired as well, such as key and fill. To keep the subject in the field of the light sources, the aerial robot is always kept oriented towards the subject. We also keep it at a fixed distance of the subject to ensure safety and a constant light intensity. The location of the subject with respect to the robot is estimated using a lidar mounted on the robot.

The characteristics of the rim light as seen from the main camera are directly related to the angle around the subject between the main camera and the light source (Fig. 5). The rim light can be made thinner by moving the robot towards the back of the subject, and it can be made wider by moving it to the front. The height of the robot also affects the rim light but does not require as much adjustment in our experience, unless subjects dramatically change pose and, e.g. go from sitting to standing. In our work, we let the photographer specify the height of the robot directly and use a standard low-level control to maintain it.

Our approach is summarized in Figure-2. We acquire video feed from the camera and compute rim-width in real-time. Rim-width is computed by looking at the silhouettes (gradients), that is, the width of the bright area across silhouettes (Section 4).

In each iteration, the rim-width is computed and compared against the desired rim-width (specified by the photographer). The difference between the measured and desired rim-widths (along with few other parameters) is used to determine the direction and magnitude of the motion of the robot. The robot is moved to the new location, and the iteration is repeated until the difference is driven to zero. In addition, we track the subject location using the lidar and ensure the proper the robot is properly oriented and positioned.

In addition to these high-level controls, we manage the subtle dynamics of quadrotor and provide high-frequency mid and low-level control. This is a well-studied problem in robotics and we rely on mostly-standard solutions, relying on a combination of onboard sensors and absolute localization provided by a motion-capture system. Future versions could replace the latter by cheaper alternatives or richer on-board sensors, but like most research on UAV control, we decided to focus on our high-level objectives and use motion capture. Out motion capture setup uses retroreflectors (small marker balls) on the quadrotor. By using an array cameras, and by triangulation, the position and orientation of the quadrotor is estimated.

4 Rim-Width Computation

Our input is an image where rim lighting dominates and we know on which side of the subject the light is (right vs. left). We identify pixels that correspond to the subject boundary that is strongly illuminated from one side and compute the width and orientation of the silhouette. Given a distribution of orientations and rim-widths, we focus on large clusters or peaks as they usually correspond to areas of the image with well-defined consistent rim lighting. We use the average width of these large rim areas as our global characterization of rim lighting. While the average rim width across the image does not claim to directly measure the aesthetic quality of rim lighting, it provides a reliable control for the photographer who can increase or decrease the desired width. Our solution is based on simple image processing and other rim width characterizations could be used as well, as long as they yield stable and predictable control of the robot.

4.1 Computing Rim Width and Orientation

We are interested in areas of the image where rim lighting is prevalent and has a consistent width that emphasizes silhouettes. For this,

we first make sure that the onboard light dominates and we slightly overexpose the image so that bright pixels correspond to rim light.

Silhouette pixels To identify silhouette pixels, we build on ideas from Harris corner detection except that we seek to identify edges and exclude corners because rim width is poorly defined for them. We also wish to focus on vertical edges because our main goal is to control the horizontal location of the aerial robot, which mostly affects rim width at vertical silhouettes. Finally, rim lighting usually locally starts at the occluding contour of the subject and stops where light is at grazing angle and the cosine term of irradiance goes to zero. We want to extract pixels corresponding to the former (silhouettes) and use the sign of the dot product between the rough 2D light direction and the image gradient.

Putting all these objectives together, we define a light-direction biased structure tensor operator $\mathcal{G}[\cdot]$ as:

$$\mathcal{G}[\cdot] = \begin{bmatrix} \left(\mathcal{L}\frac{d}{dx}\cdot\right)^2 & \left(\mathcal{L}\frac{d}{dx}\cdot\right)\left(\mathcal{L}\frac{d}{dy}\cdot\right) \\ \left(\mathcal{L}\frac{d}{dy}\cdot\right)\left(\mathcal{L}\frac{d}{dx}\cdot\right) & \left(\mathcal{L}\frac{d}{dy}\cdot\right)^2 \end{bmatrix} \quad (1)$$

where, the light-direction bias operator $\mathcal{L}[\cdot]$ emphasizes pixel gradient that are horizontal and towards the light and is defined as:

$$\mathcal{L}[dv] = \begin{vmatrix} dv \cdot L_v & if\,(dv \cdot L_v > 0) \\ 0 & elsewhere \end{vmatrix} \quad (2)$$

where L_v is a coarse 2D light vector assumed to be constant across the image (either $(1,0)$ or $(-1,0)$).

Let I_M be the input intensity image and $\mathcal{F}[\cdot]$ a low-pass filter operator. We compute the structure tensor of the input image I_G by low-pass filtering both input and output as:

$$I_G = \mathcal{F}[\mathcal{G}[\mathcal{F}[I_M]]] \quad (3)$$

Using eigen decomposition of I_G, we obtain eigenvalues and vectors as:

$$I_G(i,j) = U\Lambda U^{-1} \quad (4)$$

where Λ contains the two eigenvalues for pixel (i,j), and U contains the two eigenvectors. For each pixel, we can determine if it is a strong edge and not a corner by looking at the difference in eigenvalues. This gives us I_F, which measures the strength of the silhouette edge at each pixel:

$$I_F = \frac{(\Lambda_{1,1} - \Lambda_{2,2})}{\sqrt{(\Lambda_{1,1} + \Lambda_{2,2})} + \epsilon} \quad (5)$$

The orientation angle of the edge is given by

$$I_A = \tan^{-1}\left(\frac{U_{1,1} - \Lambda_{2,2}}{U_{2,1}}\right) \quad (6)$$

Note that, we arrange Λ and U such that $\Lambda_{1,1} \geq \Lambda_{2,2}$. ϵ is a small positive quantity to avoid divide-by-zero.

Local width Using I_F and I_A, we compute the rim width for all strong edge pixels, that is for pixels $I_F(i,j) > Threshold$. We construct a line segment $L_{i,j}$ that starts at pixel (i,j) and is directed at an angle given by $I_A(i,j)$. We sample the input image I_M along $L_{i,j}$ to obtain a 1D array of pixels. The 1D array contains a pulse that starts with high intensity and eventually falls off. We estimate the width of the pulse, which is the rim width rw corresponding to the pixel (i,j). While computing rw, we start scanning from (i,j) and continue to count the pixels until we reach a pixel value that is a certain threshold lower than the peak value encountered. The total pixels counted correspond to pulse width, or the rim width. We also store the rim orientation $ro(i,j) = I_A(i,j)$ for all pixels such that $I_F(i,j) > Threshold$. Figure 3 shows the rim widths and rim orientations for an input image.

4.2 Rim peaks and average width

The above method provides us with a distribution of rim widths and orientation and we now need to aggregate it into a single control variable that characterizes the overall rim lighting in the photo.

We observe that rim lighting is visually most salient in areas of a picture where rim width is consistent both in orientation and size. We use a simple heuristic to focus on such rim light: we extract the peaks of a 2D histogram along orientation and width (Fig. 3, right.) That is, using the rim width rw and the rim-orientation ro, we construct a 2D histogram where each bin encodes the number of pixels with a particular width and orientation. In our implementation we used 180 bins for the orientation angle in degrees and 80 bins for the widths. We identify local peaks in the histogram by first thresholding and then computing local maxima.

Finally, we compute the average width of these peaks, which provides us with our control variable $rw_{average}$. We also use the width variance $rw_{variance}$ to diagnose cases where some regions of the image have excessively large rim width compared to the average (such as the left of Fig. 4), in which case we seek to reduce the average (see Section 5.1.)

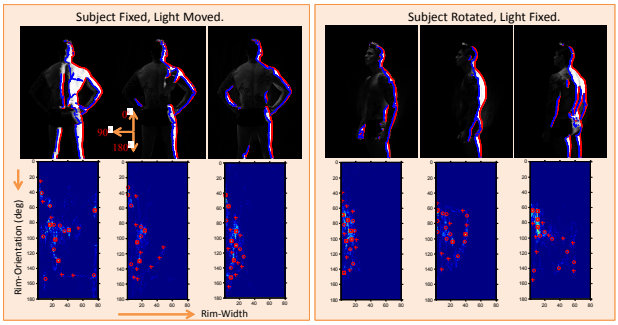

Figure 4: Left-Box: *A set of input images I_M with varying light location and fixed subject posture. From left to right, the light moves from the side to the side-rear. The corresponding histogram is plotted below. The Histogram is overlaid with markers at peak locations - a square marker indicate peaks greater than 75%, circled markers indicate peaks between 50% and 75% and + markers indicate peaks between 25% and 50%. We notice that as the light moves to the rear, the rim width becomes smaller and the peaks in the histogram cluster towards the left hand side.* **Right-Box:** *A set of input images I_M with varying subject posture and fixed light location. From left to right, the subject rotates, exposing different body curvatures, resulting in varying rim widths. The corresponding histogram is plotted below the image. We notice that a change in subject posture can dramatically change rim widths.*

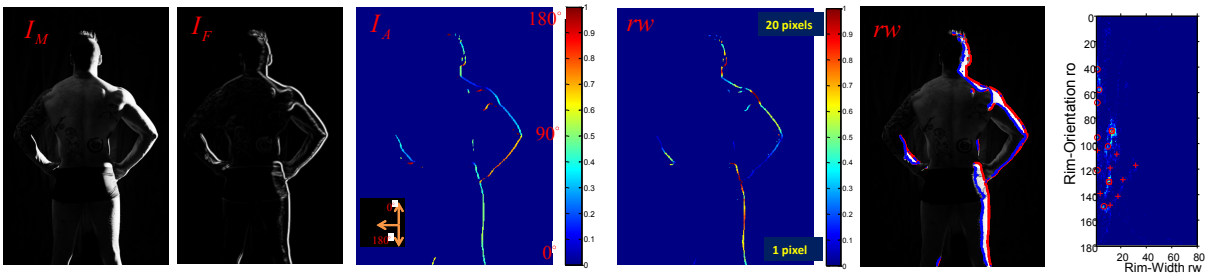

Figure 3: *Left to Right: (1) Input image I_M, (2) Boundary pixels I_F, (3) Rim orientation angle I_A, (4) rim widths rw marked on the input image I_M as color coded pixels, (5) rim widths rw marked as interior (blue) and exterior (red) points on the input image, and (6) the 2D histogram with peaks highlighted by marker. In (6) the highest peaks are marked as squares, the intermediate peaks are marked as circles, and smaller peaks are marked by $+$.*

5 Control

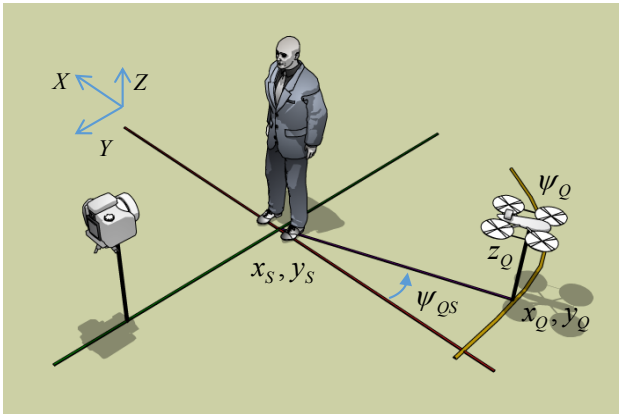

Figure 5: *Coordinate system.*

Our control strategy is motivated by a number of goals, which naturally map to the degrees of freedom of the aerial robot (Fig. 5,6), and require corresponding sensor inputs. (1) We focus on the control of the robot along a horizontal plane. (2) Our main objective is to achieve a given rim width using sensory input from the photographer's camera, which can be achieved by controlling the polar coordinate ψ_{QS} of the robot around the subject. (3) We need to make sure that the light carried by the robot is directed towards the subject, inducing a desired yaw orientation, and assessed using a robot-mounted lidar. (4) The robot must remain at a given safe distance from the subject, which is also measured by the lidar. The remaining degrees of freedom are controlled by the required constant height and the internal dynamics of the robot. In this section we use the terminology of Q, S for the quadrotor and subject respectively.

Efficient control of the delicate robot dynamics demand rich sensor inputs, that is measurement of positions, their rates and so on. Although the robot boasts a variety of sophisticated onboard sensors (gyros, accelerometers, tilt sensors, height sensors etc.), additional sensing becomes essential to ensure robustness and fast response. Because some of the onboard sensors have limited temporal rate, latency, and accuracy, we enrich these sensory data with externally located sensors (an indoor GPS). Although this may hinder portability, we trust the future technological progress in the field of state estimation will alleviate the need of external sensing. Moreover, we limited ourselves to available robot hardware with a given set of sensors.

We use a standard hierarchical control approach where our outer layer is used to control two levels of inner layers that run at increasingly higher rates and rely respectively on data about the 3D localization of the robot. Our contribution in this paper pertains to how we organize various degrees of freedom into control layers based on functional requirement and sensory data quality. This paper focuses on the outer layer, however we also cover the inner layers for completeness. We first cover the dynamics of the quadrotor aerial robot before describing its control. For a greater exposition on the dynamics and control of a quadrotor, readers may see [Lozano et al. 2005], [Bouabdallah and Siegwart 2007].

5.1 Lighting control

We first focus on the control of the quadrotor location along the horizontal plane. We will discuss other degrees of freedom in the following sections. Our objectives are best expressed in polar coordinates around the subject (Fig. 5). Let ψ_{QS} be the angle in the 2D plane between the quadrotor and the world x-axis. ψ_{QS} affects the rim width, however we also want to maintain d_{safe} distance to the subject to ensure safety as well as constant light intensity.

Angle Given the current average rim width computed from the main camera (Section 4), we need to move the aerial robot around the subject to achieve a specified width. We cannot directly compute the optimal ψ_{QS} and we only know the directions that will increase and decrease the width. This is why we use an iterative process that seeks to modify the polar angle ψ_{QS} at a speed proportional to the mismatch of rim width. At each iteration of the outer control loop, we compute the desired rate of angle change as:

$$\Delta\psi_{QS,des}(t) = k\left(rw_{average}(t) - rw_{desired}\right) \tag{7}$$

where $rw_{average}(t)$ is the average rim width at time t. $rw_{desired}$ is the desired rim width and k is a constant for numerical normalization. In addition, we use dead zoning, where we zero out the difference if it is within a small threshold (usually set at 3 pixels in our implementation) to fall back to stable hovering when the width is close enough.

If the variance of rim width is above a threshold (15 in practice), we also want to move the UAV to reduce rim width and use:

$$\Delta\psi_{QS,des}(t) = k\left(rw_{average}(t) - rw_{desired}\right) + k_2\left(rw_{variance}(t)\right) \tag{8}$$

Given this desired rate of angular change $\Delta\psi_{QS,des}$, we implement the following control law to generate the desired angle $\psi_{QS,des}$ with an integral controller:

$$\psi_{QS,des} = \int_0^t K_{adapt}\Delta\psi_{QS,des}dt \tag{9}$$

where K_{adapt} is the adaptation gain that influences how fast or slow the quadrotor moves in response to the input $\Delta\psi_{QS,des}$. We add limits on the integrator that essentially restricts the quadrotor from entering the field of view of the camera as it goes around the subject. Large K_{adapt} means quadrotor adapts quickly, but at the expense of overshooting and ringing, which is a natural consequence of dynamics. While this issue may be a problem for continuous adaptation, we used this as a optional feature. Instead of allowing the quadrotor to settle to it optimal point, we trigger the camera automatically when the quadrotor passes the optimal point, and then use the post-capture time (when the photographer is reviewing the photograph) to allow the quadrotor settle in the optimal position.

Distance and location Using the lidar, we estimate the position of the subject in the quadrotor reference frame and translate it to world frame to obtain x_S, y_S. The algorithm for subject detection is based on template matching, a standard approach. Our goal now is to achieve and maintain a fixed distance d_{safe} from the subject. Along with the subject position, the desired angle $\psi_{QS,des}$ and d_{safe} provide us with the next desired 2D position of the robot $x_{Q,des}, y_{Q,des}$:

$$\begin{bmatrix} x_{Q,des} \\ y_{Q,des} \end{bmatrix} = \begin{bmatrix} x_S + d_{safe}\cos\left(\psi_{QS,des}\right) \\ y_S + d_{safe}\sin\left(\psi_{QS,des}\right) \end{bmatrix} \tag{10}$$

In the event of subject position not being detected, previously known position of the subject is used (dead reckoning). To avoid collision with any object in general, an internal guard-band violation from lidar triggers an emergency landing.

5.2 Low-level control

Each iteration of the outer loop provides a desired 2D location. With the addition of the specified height and the yaw that aligns the quadrotor with the subject, this specifies the four actuated degrees of freedom of the quadrotor. The intermediate loop uses data about the current localization and orientation of the quadrotor (provided by the motion capture system and the onboard sensors) to guide the robot towards this 3D point and orientation. This is a standard robotics task, albeit challenging because the system has an unstable dynamics and is under actuated. We include our control strategy below for completeness but it mostly follows standard robotics approaches. The reader who is not interested in low level control issues can directly skip to Section 5.3

Simplified Dynamics of a Quadrotor A quadrotor consists of a rigid frame with four propellers (actuators) that in combination produce a thrust force F_{zb} along its body z-axis, and three body torques (rotation forces) M_ϕ, M_θ, M_ψ. These forces are electronically controlled in order to make the quadrotor follow a desired motion, or hover at a fixed 3D location. Since the quadrotor has 6 degrees of freedom, that is, position x_Q, y_Q, z_Q and Euler rotation angles ϕ_Q, θ_Q, ψ_Q, and only 4 force inputs, we can control only 4 of the 6 degrees simultaneously. This leads to a well known problem of underactuatedness, thus demanding a challenging control design. The control inputs M_ϕ, M_θ, M_ψ directly influence respectively the angles ϕ_Q, θ_Q, ψ_Q, also known as roll, pitch and yaw. This is illustrated in Figure-6. There is no direct control of x-y motion from the input, instead, this is achieved by controlling the internal variables ϕ_Q and θ_Q.

The approximate rotational dynamics of the quadrotor can be summarized as

$$\begin{bmatrix} \ddot{\phi} \\ \ddot{\theta} \\ \ddot{\psi} \end{bmatrix} \approx \begin{bmatrix} \frac{1}{J_x} M_\phi \\ \frac{1}{J_y} M_\theta \\ \frac{1}{J_z} M_\psi \end{bmatrix} \tag{11}$$

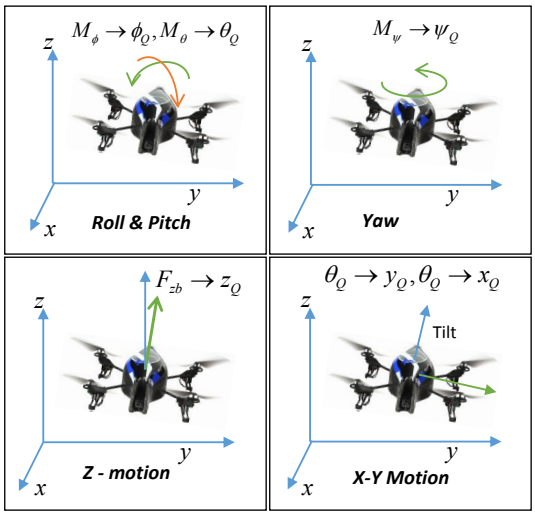

Figure 6: *Quadrotor motion as a result of various control inputs.*

where $J_{x,y,z}$ are the moment of inertia of the quadrotor. The dynamics along the z-axis is given by

$$\ddot{z}_Q \approx -g + \left(\cos\phi_Q \cos\theta_Q\right)\frac{F_{zb}}{m_Q} \tag{12}$$

where g is the acceleration due to gravity, and m_Q is the mass of the quadrotor. As mentioned earlier the horizontal x-y dynamics depend on the rotational dynamics and not directly on the control input, and this can be written as

$$\begin{bmatrix} \ddot{x}_Q \\ \ddot{y}_Q \end{bmatrix} \approx \begin{bmatrix} \cos\psi_Q & -\sin\psi_Q \\ \sin\psi_Q & \cos\psi_Q \end{bmatrix} \begin{bmatrix} g\theta_Q \\ -g\phi_Q \end{bmatrix} \tag{13}$$

Intermediate Loop Control Systems Here we describe the control of x-y position of the quadrotor with reference to the subject. Given equation 13, we control ϕ_Q and θ_Q in order to control x_Q and y_Q as follows

$$\begin{bmatrix} \theta_{Q,des} \\ \phi_{Q,des} \end{bmatrix} = \begin{bmatrix} \cos\psi_Q & \sin\psi_Q \\ -\sin\psi_Q & \cos\psi_Q \end{bmatrix} \begin{bmatrix} C_{PID}\left(x_{Q,des} - x_Q\right) \\ C_{PID}\left(y_{Q,des} - y_Q\right) \end{bmatrix} \tag{14}$$

Inner Loop Control Systems The structure of the inner loop rotation controllers is given by

$$\begin{bmatrix} M_\phi \\ M_\theta \\ M_\psi \end{bmatrix} = \begin{bmatrix} C_{PID}\left(\phi_{Q,des} - \phi_Q\right) \\ C_{PID}\left(\theta_{Q,des} - \theta_Q\right) \\ C_{PID}\left(\psi_{Q,des} - \psi_Q\right) \end{bmatrix} \tag{15}$$

where, the proportional-integral-derivative (PID) controller is defined by

$$C_{PID}\left(e\right) = eK_P + K_I \int_{-\infty}^{t} edt + \dot{e}K_D \tag{16}$$

where, K_P, K_I, K_D are control gains that indicate how the error e influences the correction forces. The subscript $_{des}$ denotes the desired quantity that we want the quadrotor to take. Except for ψ_Q, all measurements are made with onboard sensors. The height of the quadrotor is controlled using

$$F_{zb} = \frac{m_Q g + C_{PID}\left(z_{Q,des} - z_Q\right)}{\cos\theta_Q \cos\phi_Q} \tag{17}$$

The height measurement z_Q is usually done using the ultrasonic distance sensor on the quadrotor. In the event of unreliable height sensing, external measurements of z_Q are used.

5.3 Aggressive control mode

We implemented two modes of operation: (1) Continuous mode and (2) Aggressive, autotrigger mode. In continuous mode, the quadrotor continuously adapts to the changes in subject posture and viewpoint. When the subject makes a sudden posture changes, the photographer has to wait until the quadrotor moves to the new location (which may be on the order of 1 to 2 second in extreme cases) and then take a photograph. In mode (2), the photographer presses the shutter button half-way through (a standard feature in professional cameras that starts auto-focusing, etc.), which we recognize and use to initiate the quadrotor motion. In this case we set the gain factor, K_{adapt} in equation-9, to a much higher value which causes the quadrotor to move very fast but over shoot. The instant when quadrotor passes through the optimal location, we automatically trigger the camera capturing the photograph. We then allow the quadrotor to over shoot, slow down, and settle to the optimal point. The hardware we developed to sense the half-press of the shutter button, and to trigger the camera involves a microcontroller that communicates with the *remote-trigger* port of the camera.

6 Results

We demonstrate our approach on various subjects including a plastic mannequin, and male and female models with varied clothing. We show photographic results, as well as experimental plots to validate our approach.

Figure 7: *Photographic results optimized for average rim width. For $rw_{desired} = 9$, the lighting optimization resulted in $rw_{average} = 7.2$ in the case of the left image, and $rw_{average} = 11.5$ in the case of the right image.*

6.1 Performance

The rim computation was performed at $\sim 23fps$ while the quadrotor onboard inner loop controller ran at around $\sim 200fps$. The intermediate loop ran at around $\sim 60 - 100fps$ and the lidar provided depth scans at $\sim 10fps$. The height of the quadrotor was chosen to be between $750mm - 1200mm$, depending on the photographer's choice.

6.2 Photographic Results

Figure-1 (top row) shows photographs captured for various desired rim width $rw_{desired}$ settings. Figure-7 shows results for the same $rw_{desired}$, where the aerial robot achieved the desired width within 2-3 pixel tolerance.

Figure-8 shows a female subject in sitting position, performing a yoga posture. In the second and third image, $rw_{desired}$ is the same but we notice that a change in posture has made the quadrotor shift to a new location. A female subject in figure-9 performs several postures, both in upright and sitting position.

Figure 9: *A female model performs several ballet poses. The photographer chose to have the same $rw_{desired} = 10$ for all the above images. A fill light was also triggered during the capture process. The image on the top left was captured in aggressive, auto trigger mode, while the rest were captured in continuous adaptation mode.*

Figure-10 shows a subject with clothing that is not tight against

Figure 8: *Left: A subject performing yoga postures. When the subject changed in the posture from what is shown in the center image to what is shown in the right image, the quadrotor moved to a new optimal location, traveling about a meter. In the center image, the rim on the torso dominated and hence the quadrotor had to move back to reduce the average width. However, in the right image, where the legs are upward folded, thinner rims now caused the average rim width to drop, as a result, the quadrotor moved forward. Notice how the torso is over lit in the right image. This is a consequence of wide range of curvatures in the subject.*

their body. The second photograph shows the subject with a large camera lens. Because the lens is much brighter and has a well defined geometry, the histogram has very few peaks. In this case, the photographer specified the desired peak location for the rim-width optimization.

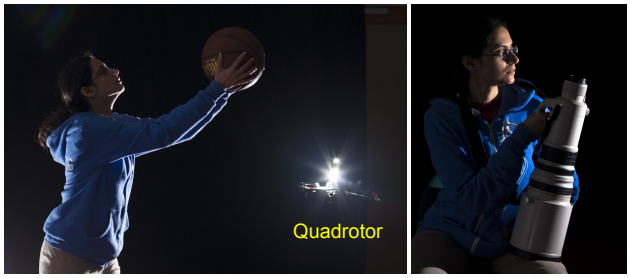

Figure 10: *Left: Subject with clothing that is not tight. Right: the subject holding a lens, which cased a strong dominant rim by setting* $rw_{desired} = 20$*, with actual achieved* $rw_{average} = 17$.

6.3 Technical Evaluation

Evaluation of Repeatability. We fix the camera and the mannequin subject, and $rw_{desired}$, and conduct several experimental trials starting the quadrotor (hovering at fixed height) with the same initial position of $\psi_{QS} = 60deg$. We then start the optimization process and record the angle ψ_{QS} when the quadrotor reached the optimal location, that is when $rw_{desired} \approx rw_{average}$. Figure 11 shows the final angles achieved. We observe that the robot consistently reached the same location within a tolerance of ± 5 degrees.

Evaluation of Continuous Adaptation. In this experiment, we fixed the camera and allowed the quadrotor to continuously adapt to the changing posture of the subject. We rotated the mannequin by minimally interfering with the scene. We evaluated two types of motion, slow and jerky, as indicated in Figure 12. For this experiment, the photographer indicated that a tolerance of ± 3 pixels was acceptable.

With the jerky motion, the quadrotor quickly returns to the optimal location in about $2sec$. For small motions of the mannequin, the quadrotor tracked the change, and adapted its location to maintain a constant rim width (within the specified tolerance range).

Adaptation to Changes in Viewpoint. In the following experiment, a female model posed while the photographer moved between positions C_1 and C_2 as shown in figure-13. The change in viewpoint caused a change in lighting effect as seen from the camera. The robot responded to this change automatically and continuously moved from Q_1 and Q_2 in order to maintain the same desired average rim width. This result demonstrates our system's capability to adapt to motion of the photographer.

6.4 Discussion and limitations

We have demonstrated a proof-of-concept system that can achieve a desired rim effect but there are several potential improvements.

Energy Efficiency. While we used a continuous light source, a more energy efficient approach is to use pulses of light that are synchronized with the camera. This may save significant amount of energy, which is a vital resource on an aerial robot. Lidar consumes only a fraction of energy and may not be a bottleneck.

Light modifiers. It would be worthwhile to attach suitable light modifiers that are lightweight, and that can aerodynamically conform to the aerial robot to enhance the quality of photographs.

Flash Power. The size of the flash strobe is only limited by the payload capacity of the aerial robot. Although we used a very light and low cost aerial robot, a little additional cost can provide higher payload capacity. For instance, it is typical to have 0.5-1kg of payload even with inexpensive quadrotors ($1000).

Outdoor Usage. One issue of using our system outdoors is the presence of background. In order to evaluate the influence of our light on the subject, we need to remove the background. One possible way to suppress the background is to take two photographs in quick succession, one with a powerful flash strobe and another no-flash image, and then use the difference image to suppress the background.

Outdoor Localization. In our setup, we used an indoor localization system to obtain some of the quadrotor measurements. In outdoors, by combining lidar data with global positioning data, and a magnetometer, one could still use the same control law. However, since these measurements are available at a low rate, the whole system may be slower. Another alternative is to setup a portable

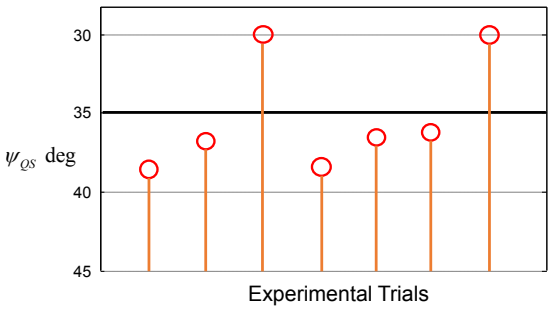

Figure 11: *Starting from the same initial location of $\psi_{QS} = 60deg$, the quadrotor reached roughly to the same spot for several trials. The camera and subject remained fixed. The mean is computed to be $35deg$ and variance 12. In each case the quadrotor moved to the optimal point in about 2.4 seconds, with an average speed of $30deg/sec$.*

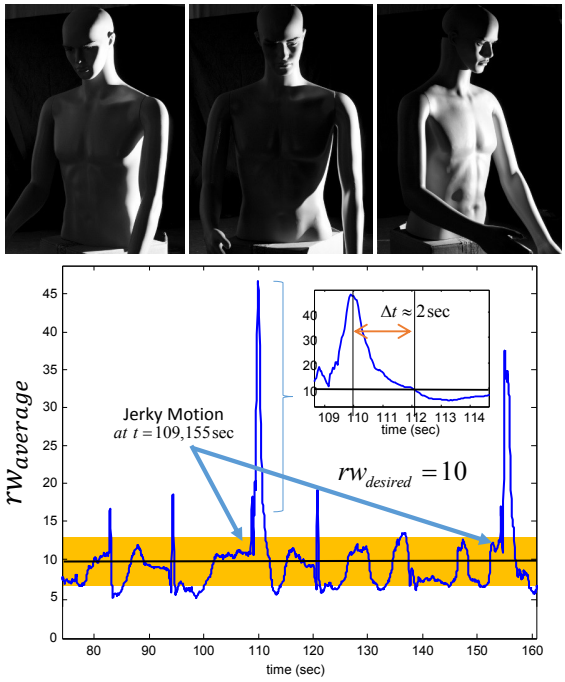

Figure 12: *Plot of rim width $rw_{average}$ vs. time as the mannequin is rotated about it's center. With $rw_{desired} = 10$, we note that the quadrotor constantly tried to bring the $rw_{average}$ towards $rw_{desired} = 10$. In the extreme cases when the mannequin was rotated by over $45deg$ with a jerky motion at $t = 109sec$, indicated by a strong peak in the plot, the quadrotor moved to the optimal location within about $2sec$. In cases when the mannequin was moved gently, the quadrotor kept pace and constantly adapted. The small deviations from $rw_{desired} = 10$ can be attributed to both the specified tolerance, as indicated by the yellow band, and the quadrotor's noisy motions. The top row of images (not rim width optimized) show some of positions of the mannequin during the experiment.*

motion capture system which can be deployed outdoors with setup time comparable to the setup time of four portable studio lights.

Other Platforms and lighting objectives. Our pipeline focused on rim-lighting optimization and the use of a quadrotor. However, both ends of this pipeline can be a variable. For instance, one could use a Roomba-like wheeled robot to perform a similar function, perhaps with significantly higher payload capacity. One could also explore using aerial robots for other styles of lighting, for instance, back lighting and key lighting.

Variance in curvature For complex geometries with a wide range of curvatures, any given light might not achieve a single rim width for all parts of the object. Reasonable rim widths on thinner parts, over expose thicker parts; while reasonable rim widths on thick parts mean the thin parts do not receive light at all. To address this issue in the case of static or near-static subjects, we prototyped an approach takes a number of images with varying light locations (that is, for various ψ_{QS}) and composite them by selecting regions from each image that have a satisfactory rim widths (Figure 14). For each image we automatically generate matte masks, and automatically blend the images together. By imposing a soft constraint on the desired rim width, we avoid generating artificial look. We captured still images at 14fps; the flash was hand held, and was synchronously triggered at 14fps.

7 Conclusions

This paper presents a new approach to computational illumination where light sources are actuated and automatically adjusted to the view from the photographer's camera, which allows lighting to react in real time to changes in viewpoint, subject location, and pose. Our new rim lighting scheme handles dynamic subjects and relies on an aerial robot as a light carrying platform. We propose a new lighting control system based on the collaboration between the aerial robot and the main camera that achieves and maintains given rim lighting characteristics under changes in subject posture and position, and camera movement. Using an aerial robot, a quadrotor, and a few off-the-shelf components, we demonstrate our approach on a variety of subjects. We believe that such a combination of computational photography, image analysis, and robotically-actuated computational illumination can provide photographers with greater flexibility in dynamic situations and dramatically reduce the need for a full crew of assistants.

References

AKERS, D., LOSASSO, F., KLINGNER, J., AGRAWALA, M., RICK, J., AND HANRAHAN, P. 2003. Conveying shape and features with image-based relighting. In *Proceedings of the 14th IEEE Visualization 2003 (VIS'03)*, IEEE Computer Society, 46.

ANRYS, F., DUTRÉ, P., AND WILLEMS, Y. 2004. Image based lighting design. In *4th IASTED International Conference on Visualization, Imaging, and Image Processing*.

BOUABDALLAH, S., AND SIEGWART, R. 2007. Full control of a quadrotor. In *Intelligent robots and systems, 2007. IROS 2007. IEEE/RSJ international conference on*, IEEE, 153–158.

BOUSSEAU, A., CHAPOULIE, E., RAMAMOORTHI, R., AND AGRAWALA, M. 2011. Optimizing environment maps for material depiction. In *Computer Graphics Forum*, vol. 30, Wiley Online Library, 1171–1180.

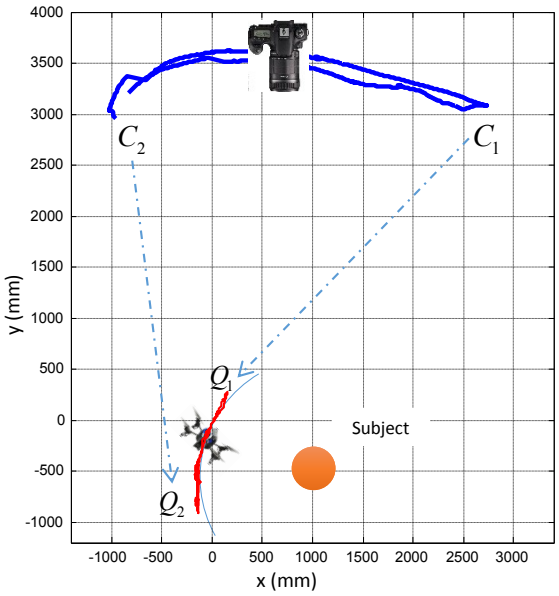

Figure 13: *The top view shows the $x - y$ trajectory of the camera and the robot. A female subject performed gentle posture changes while the photographer moved between positions C_1 and C_2, shown in the blue trajectory. To maintain a consistent average rim width, the robot moved between Q_1 and Q_2, shown in red. The circle represents the subject's location. All distances are in mm.*

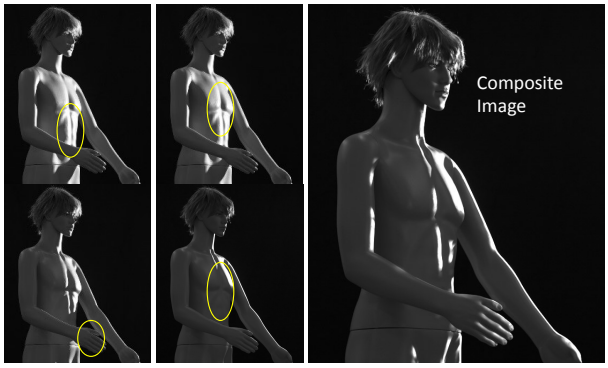

Figure 14: *Smaller images on the left are a subset of images captured with varying light position. Notice the variation of rim widths because of the wide range of curvatures within a given input image. The yellow ellipses show the regions of the image that either have excessive or no rim at all. The larger image on the right is a semi-automatically composited rim image using around 20 images.*

BOYADZHIEV, I., PARIS, S., AND BALA, K. 2013. User-assisted image compositing for photographic lighting. *ACM Trans. Graph. 32*, 4 (July), 36:1–36:12.

BRISTEAU, P., CALLOU, F., VISSIÈRE, D., PETIT, N., ET AL. 2011. The navigation and control technology inside the ar. drone micro uav. In *World Congress*, vol. 18, 1477–1484.

DEBEVEC, P., WENGER, A., TCHOU, C., GARDNER, A., WAESE, J., AND HAWKINS, T. 2002. *A lighting reproduction approach to live-action compositing*, vol. 21. ACM.

EISEMANN, E., AND DURAND, F. 2004. Flash photography enhancement via intrinsic relighting. In *ACM Transactions on Graphics (TOG)*, vol. 23, ACM, 673–678.

LOZANO, R., CASTILLO, P., AND DZUL, A., 2005. Modeling and control of mini-flying machines.

MOHAN, A., TUMBLIN, J., BODENHEIMER, B., GRIMM, C., AND BAILEY, R. 2005. Table-top computed lighting for practical digital photography. In *Rendering Techniques 2005: 16th Eurographics Workshop on Rendering*, 165–172.

PARROT, 2010. AR Drone Quadrotor. `http://en.wikipedia.org/wiki/Parrot_AR.Drone`. [Online;].

PELLACINI, F., BATTAGLIA, F., MORLEY, R., AND FINKELSTEIN, A. 2007. Lighting with paint. *ACM Transactions on Graphics (TOG) 26*, 2, 9.

PETSCHNIGG, G., SZELISKI, R., AGRAWALA, M., COHEN, M. F., HOPPE, H., AND TOYAMA, K. 2004. Digital photography with flash and no-flash image pairs. *ACM Trans. Graph 23*, 3, 664–672.

POULIN, P., AND FOURNIER, A. 1992. Lights from highlights and shadows. In *Proceedings of the 1992 symposium on Interactive 3D graphics*, ACM, 31–38.

RASKAR, R., TAN, K., FERIS, R., YU, J., AND TURK, M. 2004. Non-photorealistic camera: depth edge detection and stylized rendering using multi-flash imaging. In *ACM Transactions on Graphics (TOG)*, vol. 23, ACM, 679–688.

SCHOENEMAN, C., DORSEY, J., SMITS, B., ARVO, J., AND GREENBERG, D. 1993. Painting with light. In *Proceedings of the 20th annual conference on Computer graphics and interactive techniques*, ACM, 143–146.

WANG, O., FUCHS, M., FUCHS, C., DAVIS, J., SEIDEL, H.-P., AND LENSCH, H. 2010. A context-aware light source. In *IEEE International Conference on Computational Photography*, IEEE.